General Disclaimer

One or more of the Following Statements may affect this Document

- This document has been reproduced from the best copy furnished by the organizational source. It is being released in the interest of making available as much information as possible.

- This document may contain data, which exceeds the sheet parameters. It was furnished in this condition by the organizational source and is the best copy available.

- This document may contain tone-on-tone or color graphs, charts and/or pictures, which have been reproduced in black and white.

- This document is paginated as submitted by the original source.

- Portions of this document are not fully legible due to the historical nature of some of the material. However, it is the best reproduction available from the original submission.

Produced by the NASA Center for Aerospace Information (CASI)

SEP 83
RECEIVED
NASA STI FACILITY
ACCESS DEPT.

file
R.R.C

AN ANALYTICAL INVESTIGATION OF NO_x CONTROL TECHNIQUES FOR METHANOL FUELED SPARK IGNITION ENGINES

L.H. Browning and L.A. Argenbright
University of Santa Clara, Santa Clara, California, USA

4/82

[illegible]
9·21·82

Abstract

A thermokinetic SI engine simulation was used to study the effects of simple NO_x control techniques on performance and emissions of a methanol fueled engine. As part of this simulation, a ring crevice storage model was formulated to predict UBF emissions. The study included spark retard, two methods of compression ratio increase and EGR. The study concludes that use of EGR in high turbulence, high compression engines will both maximize power and thermal efficiency while minimizing harmful exhaust pollutants.

INTRODUCTION

Alcohol fuels are rapidly gaining popularity as excellent alternatives to petroleum fuels throughout the world. Studies in our laboratories have shown alcohols to be superior to gasoline in performance, emissions, health and safety [1,2].* Continuing research and vehicle fleet studies define problem areas which need to be solved before alcohol fuels are ready for public use. A united world effort will continue to reduce these problem areas such that alcohols can be safely introduced into the marketplace without concern for larger problems downstream.

While alcohol fuels are generally clean burning, air pollution problems existing in major cities throughout the world will require emissions controls on all combustion sources. Since oxides of nitrogen (NO_x) emissions are fundamental in the formation of photochemical smog and are the hardest emission to control, a review of simple NO_x control techniques is presented in this paper. With this study, a simple method of NO_x control can be defined without large penalties in performance or exhaust emissions.

The method used in this paper to study these NO_x control techniques is a fundamental spark ignition (SI) engine computer model. This approach is used since the interaction between engine design and operating variables is sufficiently complex that a fundamental model is essential in interpreting performance and emissions results from a spark ignition engine. A fundamental model employs current knowledge and semi-empirical formulations of combustion and pollutant formation processes occurring during an SI engine cycle to predict, in a reasonably expedient and low-cost fashion, the results of various changes in engine design and operating variables. The results from this kind of study can be used to guide experimentalists in interpreting their results and engine designers in screening various concepts in engine design prior to expensive hardware development and testing.

THE COMPUTER MODEL

The computer model used in this study has been under continuous development for the past ten years. During this time, various highlights of this model have been presented in the literature [3,4,5]. The model is a combination of

---

*Numbers in brackets [] denotes references listed at end of paper.

(NASA-CR-172847) AN ANALYTICAL
INVESTIGATION OF NO SUB X CONTROL TECHNIQUES
FOR METHANOL FUELED SPARK IGNITION ENGINES
(Santa Clara Univ.) 8 p HC A02/MF A01
CSCL 13I G3/37
N83-33168
Unclas
36451

two submodels, the kinetic Otto cycle submodel and the kinetic exhaust submodel. The kinetic Otto cycle submodel includes both thermodynamic and chemical kinetic considerations of processes occurring during the intake, compression, combustion and expansion phases of the actual SI engine cycle. Its details are published in Reference 3. Modification of the model to incorporate squish chamber cylinder head geometry is outlined in Reference 4. This model uses the detailed high-temperature chemical kinetic reaction mechanism listed in Table I to define methanol oxidation, and carbon monoxide (CO) and NO_x pollutant emissions formation which occur during the combustion and expansion phases of the engine cycle.

The kinetic exhaust submodel is a one-dimensional fluid mechanics model of the exhaust port and manifold, and applies a detailed low-temperature kinetic reaction mechanism to predict unburned fuel (UBF) oxidation and aldehyde (ALD) formation during the exhaust event. The details of this model are discussed in Reference 5. The low-temperature reaction set uses all the reactions in the high temperature reaction set; however, reaction rates for reactions 24 through 28 have been replaced with those listed in Table II to better predict aldehyde oxidation at low temperatures and two additional NO_x reactions have been added to better predict NO_2 formation during the exhaust stroke (also listed in Table II).

Further refinements to the kinetic exhaust submodel result from recently published papers on hydrocarbon quench layer content [6,7,8]. These studies suggest that under normal operating conditions, wall quenching is not an important source of exhaust hydrocarbons. This is due to rapid diffusion and burn-up of quenched hydrocarbons on a millisecond time scale without formation of significant aldehydes [7]. These studies believe that exhaust hydrocarbons result from ring crevice storage and absorption-desorption of hydrocarbons in the lubricating oil. Earlier studies by Wentworth have shown up to 74% reductions in exhaust hydrocarbon concentrations by eliminating the ring crevice [9]. Thus, a submodel utilizing ring crevice storage was formulated to calculate input hydrocarbon concentrations for the kinetic exhaust model. This ring crevice storage model assumes that half of the unburned fuel existing in the ring crevice at the end of combustion exits the crevice during the expansion stroke and is subsequently burned up on the bulk cylinder gases before the exhaust valve opens. It is also assumed that 10% of the unburned fuel in the crevice does not exit the engine cylinder during the exhaust event. The remaining 40% exits the cylinder under the following assumptions. One-half of the exiting unburned fuel is evenly entrained in the bulk cylinder flow during the time 90% of the cylinder charge (minus exhaust residual) is exhausted from the cylinder. The remaining half exits the cylinder with the remaining 10% of the bulk cylinder charge but at five times the concentration level. These assumptions result in exiting hydrocarbon concentration profiles found in experimental studies [10,11].

The method above was used in calculating input hydrocarbon levels for the exhaust model in all but the exhaust gas recirculation (EGR) study. In this part of the study, additional sources of unburned fuel emissions needed to be considered. One such source resulted from reducing manifold vacuum as EGR was added to maintain the same volumetric efficiency (η_V). This tends to increase fuel flow through the cylinder during the valve overlap period due to scavenging. Also as EGR is added, there is a general degradation from good burns to slow burns [12], thereby increasing unburned fuel emissions. Calculations using only ring crevice volume resulted in decreasing input hydrocarbon concentrations with increasing EGR. Thus for this part of the study, the input hydrocarbon concentration was calculated for the no EGR case using the ring crevice model and then used for all EGR addition cases as well.

Run times for the entire engine cycle simulation were typically 1100 seconds on a CDC 7600 computer. This provided the best compromise between computer time and numerical accuracy.

MODEL TUNING AND VERIFICATION

In order to tune the computer model's semi-empirical equations, experimental data was taken from the four-cylinder 2.3 liter Ford Pinto engine used by the University of Santa Clara in methanol characterization studies under federally funded grants [1,2]. The specifications for this engine are given in Table III. Cylinder number one of this engine was instrumented with a model 601B Kistler pressure transducer mounted in a model 640 spark plug adapter and connected to a model 504E charge amplifier and a Tektronix model 5011 storage oscilliscope. Exhaust emissions were taken at the cylinder's exhaust port and analyzed.

The corrected pressure trace obtained from the engine was then used to determine coefficients for both the flame speed and heat transfer equations. As shown in Figure 1, good agreement was reached between the computer model and actual pressure diagram in combustion rate; however, the model tended to predict higher peak pressures than the actual pressure trace.

Two test points are compared against the model's predictions in Table IV. The first ($\Phi = 0.9$, CR = 8.44)* represents the test conditions at which the cylinder pressure trace shown in Figure 1 was taken. The second ($\Phi = 1.0$, CR = 9.0) represents the base engine operating condition used in the parametric study. Both comparisions show good agreement in performance and emissions predictions with the actual experimental data. Predicted CO emissions, however, were much lower than actual values.

SPARK RETARD EFFECTS

In a spark ignition engine, spark timing has a large influence on the combustion process and, thus, on power, thermal efficiency (η_{th}) and emissions. As shown in Figure 2, NO_x emissions decrease rapidly as the spark is retarded from MBT (minimum spark advance for best torque) due to burning later in the cycle and, thus, at lower peak temperatures and pressures. CO emissions tended to decrease with spark retard due to higher temperatures during the expansion stroke. Unburned fuel emissions also tend to decrease with spark retard due to higher exhaust temperatures. Aldehydes, however, peak slightly retarded of MBT, then decrease with more retard. While the increasing exhaust temperatures tend to react more unburned fuel into aldehydes as the spark is retarded, the amount of unburned fuel in the ring crevice decreases with spark retard due to lower peak pressures. The latter becomes the overriding effect slighly retarded of MBT, thereby causing the aldehyde emissions to drop as the spark is retarded further. Pischinger [19] found similar results for lean mixtures, but found a steady increase in aldehyde emissions with spark retard for rich mixtures.

COMPRESSION RATIO EFFECTS

Due to the high octane rating of methanol, higher compression ratios can be used without fear of engine knock. In conventional engines, squish chamber combustion chamber geometry is used to minimize the pressure rise rate during both the start and end of combustion. Reducing the pressure rise rate during the start of combustion, which occurs during the compression stroke, minimizes the negative work. Reducing the pressure rise rate at the end of combustion minimizes the possibility of knock by minimizing end gas heating.

---

* Φ denotes fuel-air equivalence ratio while CR denotes compression ratio.

In this study, two methods of raising compression ratio are examined. The first method maintains the same open-to-squish chamber volume ratio at top center (TC) while compression ratio is raised. This maintains the same relative squish velocities with varying compression ratio and would have relatively the same effect in power and emissions as raising compression ratio in a disc chamber engine. This method is best accomplished by piston crown redesign. The second method maintains the same squish chamber clearance height while compression ratio is raised. Thus, compression ratio is raised by lowering only the open chamber height. This results in decreased squish velocities as compression ratio is raised (in comparison to method one), thereby reducing overall in-cylinder turbulence levels. This method is normally accomplished by milling the cylinder head.

With the first method, NO_x increases 29.6% by increasing the compression ratio from 9:1 to 15:1 due to higher peak pressures and temperatures as shown in Figure 3. Unburned fuel emissions rose 108.5% for the same comparison due to increased ring crevice storage and decreasing exhaust temperatures. Aldehyde emissions, however, decreased 43.9% due to lower exhaust temperatures, thereby reacting less unburned fuel during the displacement flow period of the exhaust stroke when aldehyde emissions are generally formed [5]. CO emissions rose 31.5% for the same comparison while both power and thermal efficiency rose 14.7%.

In the second method, the reduced turbulence levels and burning rate tended to limit the increase in NO_x and CO emissions as shown in Figure 4. By raising the compression ratio from 9:1 to 15:1 by this method, NO_x emissions rose 21.8%, UBF emissions rose 109.8% and CO emissions rose 25.3%. Aldehyde emissions, however, decreased only 19.3%. The trends of aldehyde emissions with compression ratio shown in Figure 4 are similar to the trends found by Pischinger [19] using a similar method to raise compression ratio. Power and thermal efficiency rose 15% for the same compression ratio increase.

EGR EFFECTS

In this study volumetric efficiency was maintained as EGR was added. A throttled condition was chosen for this study to compensate for the increased cylinder charge due to EGR addition. Furthermore, the inlet charge temperature was allowed to rise with EGR addition due to the mixing of the hot exhaust (600°K) with the cool incoming charge (289°K). This raised inlet mixture temperature substantially from 289°K for the no EGR case to 392°K for 30% EGR addition at the 65% volumetric efficiency condition. The decrease in inlet temperature as EGR was added more than compensated for the increased burning velocities, thereby raising both power and thermal efficiency as shown in Figure 5. Both power and thermal efficiency rose 8.5% with 30% EGR over the no EGR case. NO_x emissions dropped substantially showing a 97.2% reduction for the above comparison due to lower peak cylinder temperatures and pressures. These results are consistent with other investigators [20,21]. Unburned fuel emissions increased 55.8% for the above comparison due to decreasing exhaust temperatures and oxygen concentration. This matches trends found in our laboratory [21]. These factors, however, reduced aldehyde emissions 88.3%.

CO emissions dropped 70.7% for the same comparison. The interesting point is that as the exhaust temperature decreases, more of the NO is converted to NO_2. At the no EGR case, only 8.2% of the NO_x is NO_2, while of the 30% EGR case, 49% of the NO_x is NO_2. Thus, EGR is an effective method of reducing NO_x emissions without large increases in UBF emissions while also substantially reducing CO and aldehyde emissions.

CONCLUSIONS

A thermokinetic computer model was used to study the effects of simple NO_x control techniques on performance and exhaust emissions. A ring crevice storage model was also formulated for predicting unburned fuel emissions. The study showed spark retard to be an effective method of reducing NO_x, CO and UBF emissions at the expense of power, thermal efficiency and aldehyde emissions. It was also shown that by raising compression ratio in a squish chamber engine, the rise of NO_x, and CO emissions could be limited, but not without an aldehyde emission penalty. Exhaust gas recirculation, however, was shown to be a very effective method for reducing NO_x, CO and aldehyde emissions with only a slight UBF emission penalty. It is the opinion of the authors, that use of EGR in high compression methanol fueled engines with increased turbulence to reduce cycle-to-cycle variations will both maximize power and thermal efficiency while minimizing harmful exhaust emissions.

ACKNOWLEDGEMENTS

The authors wish to thank NASA-Ames Research Center for use of their computer facilities. This work was funded through NASA-Lewis Research Center Grant NAG 3-143.

REFERENCES

1. R.K. Pefley, L.H. Browning, et al, "Characterization and Research Investigation of Methanol and Methyl Fuels," ERDA Contract No. EY-76-S-02-1258, University of Santa Clara, Report No. ME-77-2, 1977.

2. R.K. Pefley, et al, "Characterization and Research Investigation of Alcohol Fuels in Automobile Engines," Final Report, DOE Contract No. DE-AC03-78CS, University of Santa Clara Report No. ME-81-1, 1981.

3. L.H. Browning, "A Thermokinetic Combustion Process Simulation for a Methanol Fueled Spark Ignition Engine," Engineer's Degree Thesis, Stanford University, Stanford, California, 1978.

4. L.H. Browning and R.K. Pefley, "Predicted Methanol-Water Fueled SI Engine Performance and Emissions," presented at the Second International Symposium on Alcohol Fuels Technology, Wolfsburg, Germany, November, 1977.

5. L.H. Browning and R.K. Pefley, "An Analytical Study of Aldehyde Formation During the Exhaust Stroke of a Methanol-Fueled SI Engine," presented at the Fourth International Symposium on Alcohol Fuels Technology, Guaruja, Brazil, October, 1980.

6. R. Bergner, H. Eberius and H. Pokorny, "Flame Quenching and Exhaust Hydrocarbons in a Combustion Bomb as a Function of Pressure, Temperature and Equivalence Ratio for Methanol and Other Alcohols," presented at the Third International Symposium on Alcohol Fuels Technology, Asilomar, California, May, 1979.

7. C.K. Westbrook, A.A. Adamczyk and G.A. Lavoie, "A Numerical Study of Laminar Wall Quenching," presented at the Western States Section Combustion Institute Meeting, Berkeley, California, October, 1979.

8. J.A. LoRusso, E.W. Kaiser and G.A. Lavoie, "Quench Layer Contribution to Exhaust Hydrocarbons from a Spark-Ignited Engine," Combustion Science and Technology, Vol. 25, pp 121-125, 1981.

9. J.T. Wentworth, "Effects of Combustion Chamber Shape and Spark Location on Exhaust Nitric Oxide and Hydrocarbon Emissions," SAE Paper No. 740529, SAE Transactions, Vol 83, 1974.

10. W.A. Daniel and J.T. Wentworth, "Exhaust Gas Hydrocarbons--Genesis and Exodus," SAE Paper No. 686b, SAE Transactions, Vol 70, 1962.

11. R.J. Tabaczynski, J.B. Heywood and J.C. Keck, "Time Resolved Measurements of Hydrocarbon Mass Flowrate in the Exhaust of a Spark-Ignition Engine," SAE Paper No. 720112, SAE Transactions, Vol 81, 1972.

12. W.G. Rado and W.J. Johnson, "Significance of Burn Types, as Measured by Using the Spark Plugs as Ionization Probes, with respect to the Hydrocarbon Emissions Levels in S.I. Engines," SAE Paper No. 750354, 1975.

13. C.K. Westbrook and F.L. Dryer, "A Comprehensive Mechanism for Methanol Oxidation," Combustion Science and Technology, Vol 20, pp 125-140, 1979.

14. W.L. Flower, R.K. Hanson and C.H. Kruger, "Experimental Study of Nitric Oxide Decomposition by Reaction with Hydrogen," Combustion Science and Technology, Vol 15, pp 115-128, 1977.

15. J.P. Monat, R.K. Hanson and C.H. Kruger, "Shock Tube Determination of the Rate Coefficient for the Reaction $N_2 + O \rightarrow NO + N$," 17th International Symposium on Combustion, the Combustion Institute, pp 543-552, 1978.

16. M. Koshi, S. Bando, M. Saito and T. Asaba, "Dissociation of Nitric Oxide in Shock Waves," 17th International Symposium on Combustion, the Combustion Institute, pp 553-562, 1978.

17. G.M. Johnson, M.Y. Smith and M.F.R. Mulcahy, "The Presence of NO_2 in Premixed Flames," 17th International Symposium on Combustion, the Combustion Institute, pp 647-660, 1978.

18. T. Tsuboi and K. Hashimoto, "Shock Tube Study on Homogeneous Thermal Oxidation of Methanol," Combustion and Flame, Vol 42, pp 61-76, 1981.

19. F.F. Pischinger and K. Kramer, "The Influence of Engine Parameters on the Aldehyde Emissions of a Methanol Operated Four-Stroke Otto Cycle Engine," presented at the Third International Symposium on Alcohol Fuels Technology, Asilomar, California, May, 1979.

20. J.A. Harrington, "Application of a New Combustion Analysis Method in the Study of Alternate Fuel Combustion and Emission Characteristics," presented at the Symposium on Future Automotive Fuels, General Motor Research Laboratories, Warren, Michigan, October, 1975.

21. R.K. Pefley, et al., "Research and Development of Neat Alcohol Fuel Usage in Automobiles," Six-Months Progress Report, NASA-Lewis Contract No. NAG 3-143, University of Santa Clara Report No. ME-81-2, July, 1981.

Table I Important High Temperature Reactions in Methanol Oxidation

	REACTION	A	n	E	REF.
1.	$CH_3OH + M = CH_3 + OH + M$	18.50	0	80.00	13
2.	$CH_3OH + O_2 = CH_2OH + HO_2$	13.60	0	50.90	13
3.	$CH_3OH + OH = CH_2OH + H_2O$	12.60	0	2.00	13
4.	$CH_3OH + O = CH_2OH + OH$	12.20	0	2.30	13
5.	$CH_3OH + H = CH_2OH + H_2$	13.50	0	7.00	13
6.	$CH_3OH + H = CH_3 + H_2O$	12.70	0	5.30	13
7.	$CH_3OH + CH_3 = CH_2OH + CH_4$	11.30	0	9.80	13
8.	$CH_3OH + HO_2 = CH_2OH + H_2O_2$	12.80	0	19.40	13
9.	$CH_2OH + M = CH_2O + H + M$	13.40	0	29.00	13
10.	$CH_2OH + O_2 = CH_2O + HO_2$	12.00	0	6.00	13
11.	$CH_4 + M = CH_3 + H + M$	[illegible]	0	88.40	13
12.	$CH_4 + H = CH_3 + H_2$	14.10	0	11.90	13
13.	$CH_4 + OH = CH_3 + H_2O$	3.50	3.08	2.00	13
14.	$CH_4 + O = CH_3 + OH$	13.20	0	9.20	13
15.	$CH_4 + HO_2 = CH_3 + H_2O_2$	13.30	0	18.00	13
16.	$CH_3 + HO_2 = CH_3O + OH$	13.20	0	0.00	13
17.	$CH_3 + OH = CH_2O + H_2$	12.60	0	0.00	13
18.	$CH_3 + O = CH_2O + H$	14.10	0	2.00	13
19.	$CH_3 + O_2 = CH_3O + O$	13.40	0	29.00	13
20.	$CH_3 + HCO = CH_4 + CO$	11.50	0.5	6.00	13
21.	$CH_3 + HO_2 = CH_4 + O_2$	12.00	0.5	0.00	13
22.	$CH_3O + M = CH_2O + H + M$	13.70	0	0.40	13
23.	$CH_3O + O_2 = CH_2O + HO_2$	12.00	0	21.00	13
24.	$CH_2O + M = HCO + H + M$	16.70	0	6.00	13
25.	$CH_2O + OH = HCO + H_2O$	14.70	0	72.00	13
26.	$CH_2O + H = HCO + H_2$	12.60	0	6.30	13
27.	$CH_2O + O = HCO + OH$	13.70	0	3.80	13
28.	$CH_2O + HO_2 = HCO + H_2O_2$	12.00	0	4.60	13
29.	$CH_2O + CH_3 = CH_4 + HCO$	10.00	0	8.00	13
30.	$HCO + OH = CO + H_2O$	14.00	0	0.00	13
31.	$HCO + M = H + CO + M$	14.20	0	19.00	13
32.	$HCO + H = CO + H_2$	14.30	0	0.00	13
33.	$HCO + O = CO + OH$	14.00	0	0.00	13
34.	$HCO + HO_2 = CH_2O + O_2$	14.00	0	3.00	13
35.	$HCO + O_2 = CO + HO_2$	12.50	0	7.00	13
36.	$CO + OH = CO_2 + H$	7.10	1.3	-0.80	13
37.	$CO + HO_2 = CO_2 + OH$	14.00	0	23.00	13
38.	$CO + O + M = CO_2 + M$	15.80	0	4.10	13
39.	$CO_2 + O = CO + O_2$	12.40	0	43.80	13
40.	$H + O_2 = O + OH$	14.30	0	16.80	13
41.	$H_2 + O = H + OH$	10.30	1.0	8.90	13
42.	$H_2O + O = OH + OH$	13.50	0	18.40	13
43.	$H_2O + H = H_2 + OH$	14.00	0	20.30	13
44.	$H_2O_2 + OH = H_2O + HO_2$	13.00	0	1.80	13
45.	$H_2O + M = H + OH + M$	16.30	0	105.10	13
46.	$H + O_2 + M = HO_2 + M$	15.20	0	-1.00	13
47.	$HO_2 + O = OH + O_2$	13.70	0	1.00	13
48.	$HO_2 + H = OH + OH$	14.40	0	1.90	13
49.	$HO_2 + H = H_2 + O_2$	13.40	0	0.70	13
50.	$HO_2 + OH = H_2O + O_2$	13.70	0	1.00	13
51.	$H_2O_2 + O_2 = HO_2 + HO_2$	13.60	0	42.60	13
52.	$H_2O_2 + M = OH + OH + M$	17.10	0	45.50	13
53.	$H_2O_2 + H = HO_2 + H_2$	12.20	0	1.90	13
54.	$O + H + M = OH + M$	16.00	0	0.00	13
55.	$O_2 + M = O + O + M$	15.70	0	115.00	13
56.	$H_2 + M = H + H + M$	14.30	0	96.00	13
57.	$H + NO = N + OH$	14.35	0	50.50	14
58.	$O + NO = N + O_2$	9.37	1.0	38.65	15
59.	$O + N_2 = N + NO$	14.26	0	76.25	15
60.	$NO + NO = N_2O + O$	12.11	0	67.20	16
61.	$N_2O + M = N_2 + O + M$	14.15	0	51.28	15
62.	$NO + H + M = HNO + M$	15.73	0	-0.60	14
63.	$HNO + H = H_2 + NO$	11.48	0.5	2.40	14
64.	$HNO + OH = H_2O + NO$	12.48	0.5	2.40	14
65.	$NO_2 + M = NO + O + M$	16.04	0	65.00	14
66.	$NO_2 + O = NO + O_2$	13.00	0	0.596	17

Note The rate constants are of the modified Arrhenius form $10^{A}T^{n}e^{-E/RT}$ with units in sec, mol/cm³ and kcal.

ORIGINAL PAGE IS OF POOR QUALITY

Table II: Important Low Temperature Reactions

	REACTION	A	n	E	REF
24.	$CH_2O + M = HCO + H + M$	11.84	0	301.00	18
25.	$CH_2O + OH = HCO + H_2O$	14.00	0	17.00	18
26.	$CH_2O + H = HCO + H_2$	13.52	0	18.00	18
27.	$CH_2O + O = HCO + OH$	13.62	0	17.00	18
28.	$CH_2O + HO_2 = HCO + H_2O_2$	12.00	0	33.00	18
67.	$NO + HO_2 = NO_2 + OH$	13.15	0	1.40	17
68.	$NO_2 + H = NO + OH$	14.54	0	1.47	17

Note: The rate constants are of the modified Arrhenius form $10^{A}T^{n}e^{-E/RT}$ with units in sec, mol/cm³ and kcal.

Table III: Engine Specifications

Engine Type	Squish Chamber OHV
Bore	9.60 cm
Stroke	7.94 cm
Connecting Rod	13.22 cm
Intake Valve Diam/Lift	4.41 cm/1.016 cm
Opens	60° BTC
Closes	100° BTC
Exhaust Valve Diam/Lift	3.81 cm/1.016 cm
Opens	100° ATC
Closes	60° ATC
Fuel Type	Methanol
Intake Temperature	284°K
EGR Temperature	600°K
Ring Crevice Volume	0.9072 cc

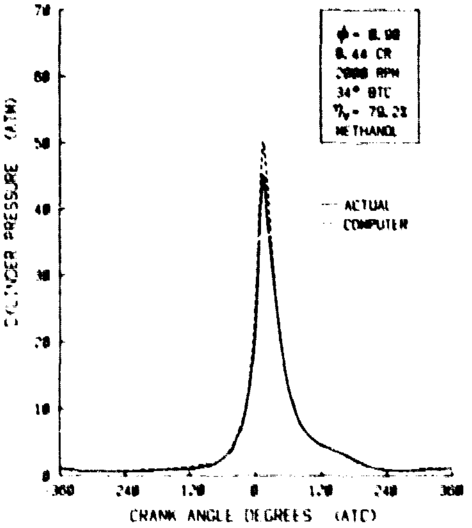

FIGURE 1: COMPARISON OF COMPUTER PREDICTED PRESSURE TRACE TO ACTUAL DATA

Table IV: Performance and Emissions Comparisons at Match Points (WOT & 2000 RPM)

	ENGINE DATA	MODEL	ENGINE DATA	MODEL
Performance:				
φ	0.90	0.90	1.00	1.00
CR	8.44	8.44	9.00	9.00
SA (°BTC)	34	34	25	25
IHP (KW)	9.84	9.76	10.70	10.81
η_{th} (%)	39.50	39.20	39.20	39.00
Emissions:				
UBF (PPM)	429	415	535	520
ALDEHYDES (PPM)	172	163	148	140
CO (%)	0.07	0.03	0.25	0.09
NO (PPM)	2413	2366	1925	1894
NO_x (PPM)	2559	2488	2042	1950

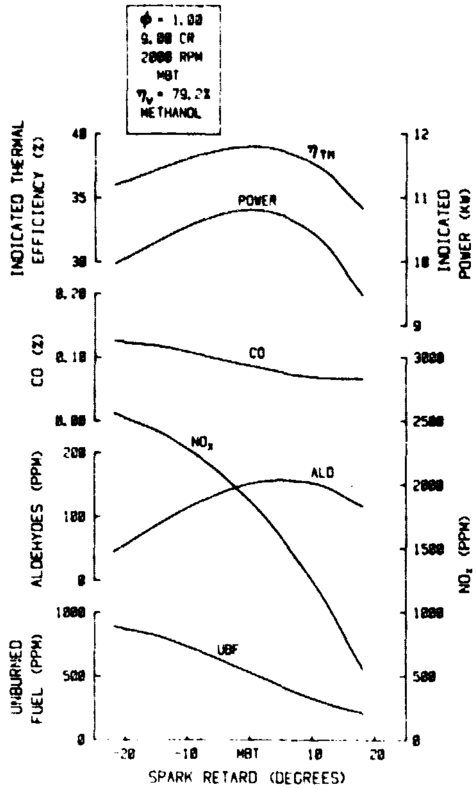

FIGURE 2: SPARK RETARD EFFECTS

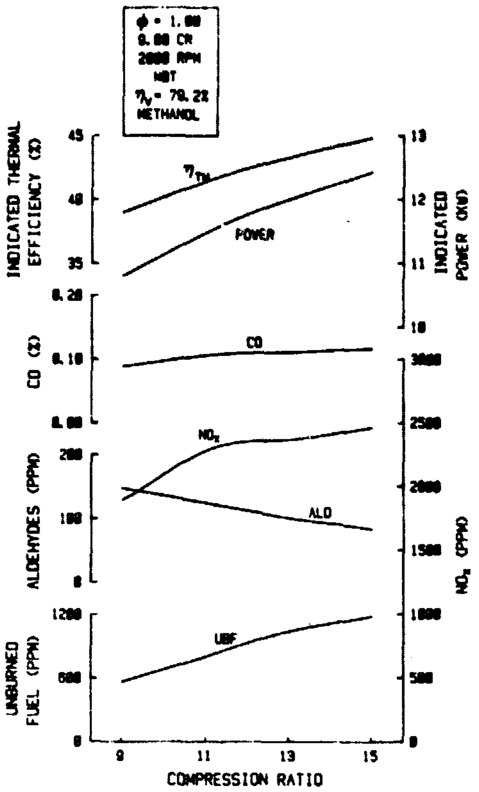

FIGURE 3: COMPRESSION RATIO EFFECTS
CONSTANT OPEN-TO-SQUISH VOLUME RATIO

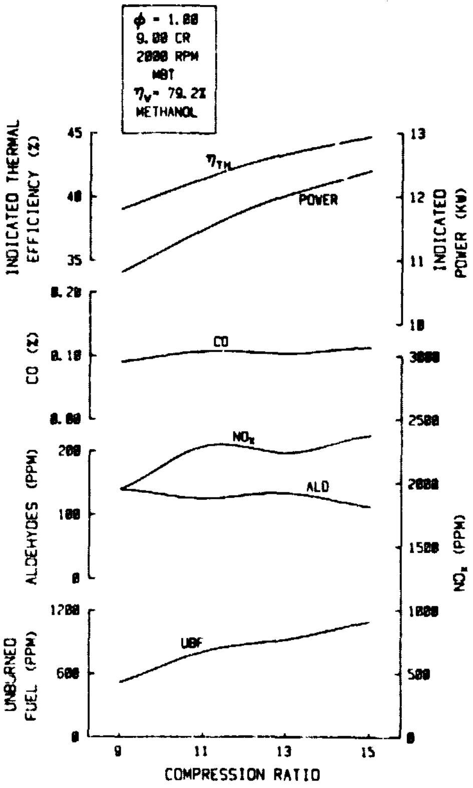

FIGURE 4: COMPRESSION RATIO EFFECTS
CONSTANT SQUISH CLEARANCE HEIGHT

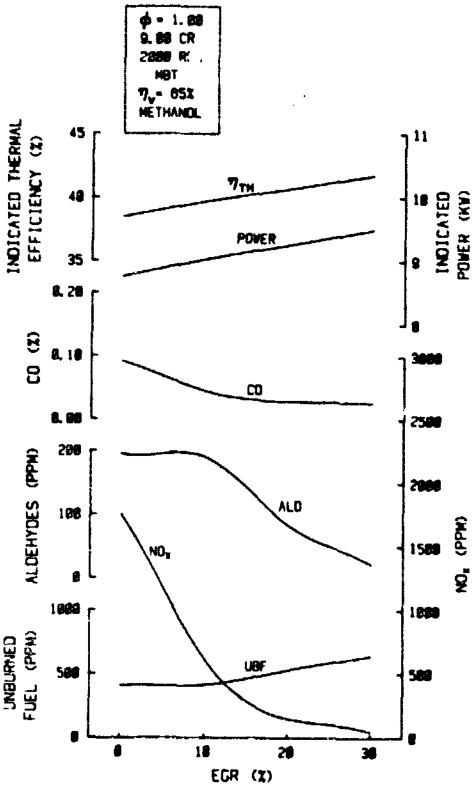

FIGURE 5: EGR EFFECTS